

Event-Conditioned Diagnostics of Kinematic, Contact, and Object-Permanence Fields in Passive Object-State World Models

Yang Liu*, Yuming Chen*

College of Intelligent Robotics and Advanced Manufacturing, Fudan University

Shanghai, China

{ly, yumingchen}@fudan.edu.cn

Abstract

World models can predict future physical states, but prediction accuracy alone does not explain how physical information is organized and used inside their latent dynamics. We introduce a controlled diagnostic protocol for studying event-conditioned latent physical structure in passive object-state world models. The protocol tests whether hidden representations encode event-regime information, whether event contexts reweight non-exclusive physical field readouts, and whether field-aligned representational components have functional consequences for prediction. Using a balanced controlled-generator dataset with free-motion, collision, and occlusion events, we evaluate recurrent, attention-based, and latent state-space transition models under a fixed-horizon forecasting setup. The models learn useful predictive dynamics and their hidden states support reliable event-regime readout. Event contexts systematically reweight kinematic, contact, and object-permanence field readouts: free motion is kinematic-dominant, collision combines kinematic and contact structure, and occlusion combines motion-related and object-permanence structure. Time-aligned and directional-consistency analyses further show phase-related shifts in field emphasis. Finally, fixed-horizon projection causal field effect (CFE) shows that suppressing field-aligned directions can degrade event-relevant prediction, with strongest evidence for contact-aligned structure in collision-contact windows and more qualified evidence for object-permanence-aligned structure in hard-occlusion hidden windows. These results support event-conditioned organization and fixed-horizon functional sensitivity of latent physical fields, while not implying explicit physical modules, isolated causal circuits, or context-invariant sliding-window generalization.

1. Introduction

World models have become a central framework for learning predictive models of physical dynamics. They compress observations into latent states and roll those states forward in time. This allows them to support planning, control, and policy learning without evaluating every decision directly in the external environment (Ha & Schmidhuber, 2018; Hafner et al., 2019; Hafner et al., 2023; Micheli et al., 2022). Early neural world models showed that agents could use learned internal simulations for control (Ha & Schmidhuber, 2018). PlaNet showed that latent dynamics can support planning from high-dimensional observations (Hafner et al., 2019). More recent Dreamer-style systems showed that learned world models can support behavior learning across diverse domains (Hafner et al., 2023). Transformer-based world models further suggest that this paradigm is not tied to a single recurrent architecture (Micheli et al., 2022). However, strong prediction or

* Equal contribution

control performance does not explain how physical information is organized inside the model. A model may predict future states accurately while representing speed, direction, contact, or object persistence in distributed and task-specific ways. These structures may not appear as explicit, factorized physical variables (Joseph et al., 2026). This motivates a shift in focus. Instead of asking only whether a world model can predict physical dynamics, we ask how physical structure is organized, reweighted, and used within latent dynamics.

Our work builds on prior progress in physical reasoning benchmarks, object-centric dynamics modeling, and representation analysis, but asks a more specific question. We move the question toward event-conditioned organization and functional use of latent physical structure. By state-conditioned, we mean that the model’s internal representation may depend not only on which physical variable is present, but also on which physical event is currently unfolding. We also treat physical fields as non-exclusive. A collision sequence still contains kinematic structure before contact, but it should place additional emphasis on contact-sensitive structure when objects interact. An occlusion sequence still contains visible motion before hiding, but it should place additional emphasis on object-permanence structure when an object becomes hidden or reappears. This distinction matters because a model that bears velocity information may still fail at collision if it does not use contact-sensitive structure, and a model that tracks visible objects may still fail at occlusion if it does not maintain hidden object state.

The remaining deeper gap is that current evaluation, modeling, and interpretability lines do not yet provide a controlled way to test how physical event context changes the organization and functional role of latent physical structure. Benchmarks tell us whether a model succeeds or fails. Object-centric dynamics models improve prediction and generalization. Probing and steering studies show that physical information can be readable or manipulable. What remains less clear is how these pieces fit together inside a world model as the physical event changes. We address this gap with a hierarchical diagnostic framework, which tests event-level separability, event-conditioned field reweighting, fixed-horizon causal sensitivity under field-aligned projection suppression, and partial time-resolved consistency under phase-aligned analyses.

2. Related Work

2.1 Physical reasoning benchmarks

Physical reasoning benchmarks make physical success and failure measurable. Physion evaluates visual physical prediction across collisions, stability, rolling, sliding, and projectile motion (Bear et al., 2021). CLEVRER focuses on collision events and asks descriptive, explanatory, predictive, and counterfactual questions about videos (Yi et al., 2019). IntPhys and IntPhys2 test violation-of-expectation judgments for intuitive-physics principles such as permanence, continuity, and solidity (Bordes et al., 2025). CATER stresses compositional actions, temporal reasoning, and object tracking under controlled scene biases (Girdhar & Ramanan, 2019). PHYRE evaluates sample-efficient physical problem solving in 2D mechanics puzzles (Bakhtin et al., 2019). These benchmarks define observable behavioral criteria for physical reasoning. But they mainly evaluate task behavior, plausibility judgments, causal question answering, or planning outcomes. They do not by themselves explain how physical information is organized inside a model.

2.2 Object-centric dynamics and world models

Object-centric dynamics models decompose scenes into objects, slots, particles, or relational state variables, and then learn how these entities evolve over time (Shamsian et al., 2020; Song et al., 2025; Villar-Corrales

et al., 2023; Wu et al., 2022). They can improve long-horizon prediction, future reasoning, visual question answering, planning, and object tracking. Some models directly target object permanence and occlusion. They learn to track hidden objects, anticipate reappearance, or maintain object-specific state through occlusion (Shamsian et al., 2020; Traub et al., 2024). Other models introduce explicit kinematic structure or separate object dynamics from object interactions (Song et al., 2025; Villar-Corrales et al., 2023). This line of work shows that object structure, kinematic structure, and interaction structure can improve prediction and generalization. Its main goal, however, is usually better rollout, better prediction, better planning, or better generalization. It is less often focused on how latent physical structure changes its organization and functional role when the physical event changes.

2.3 Probing, steering, and representation diagnostics

Internal representation analysis comes closer to our diagnostic focus. Recent interpretability studies show that physical variables can be decoded from hidden states of video or world models. Speed, acceleration, motion direction, object position, and game-state variables can become accessible in learned representations (Joseph et al., 2026; Zhang, 2026). These representations are not always simple factorized variables. For example, direction can be encoded through a distributed population geometry rather than a single explicit coordinate (Joseph et al., 2026). Other work goes beyond probing. Probe-derived Concept Activation Vectors can steer physical plausibility judgments in video world models (Alam, 2026). Interventions along probe-derived directions can also change the predictions of learned environment simulators (Zhang, 2026). Causal and contextual world-model studies further show that learned latent structure can support counterfactual dynamics, intervention-aware prediction, or context-dependent rollout behavior (Ding et al., 2026; Lei et al., 2022; Röder et al., 2026). These results show that physical information can be readable, geometrically organized, and sometimes functionally used.

3. Problem formulation

3.1 Passive Object-State World Models

In this work, we study passive object-state world models, where a model observes a sequence of object states and predicts how those states evolve over time. Each state contains object-level variables such as position, velocity, size, visibility, or other available annotations. We write the object-state sequence as $s_{1:T}$, where s_t summarizes the scene at time t . A transition model is the part of the world model that maps observed states to future states. It encodes the observed prefix into hidden states h_t , and predicts a future trajectory $\hat{s}_{t+1:t+H}$, where H is the prediction horizon. In our experiments, this prefix-horizon interface is fixed: the models observe the first eight frames and predict the next eight frames. Although this fixed-horizon setup does not test arbitrary sliding-context generalization, it provides a controlled forecasting interface in which all architectures receive the same observed prefix and are evaluated over the same future target horizon. This design makes the subsequent diagnostic comparisons more interpretable by minimizing potential confounds from differences in context length, prediction horizon, and event-aligned resampling.

The word passive means that the models considered here do not receive agent actions as input. They are not trained to choose actions, plan interventions, or control a robot. They only learn the dynamics of observed physical scenes, which makes the setting different from action-conditioned reinforcement-learning world models. Therefore, our diagnostic target is narrowed.

We use object-state inputs rather than raw pixels. This choice removes the confound of object discovery,

segmentation, and visual feature extraction. It allows us to focus on the transition dynamics themselves. The goal of this article is not to test whether a model can perceive objects from video, but to test whether, given object-level state information, the transition model organizes latent physical structure in a way that depends on the physical event context.

Although our setting is passive, it is still relevant to more general action-conditioned and control-oriented world models. Such models also rely on latent states to predict future dynamics, evaluate possible futures, or support downstream planning and control. In those settings, action selection depends on how the model represents the physical consequences of states and actions. Though a passive transition model does not choose actions, it provides a controlled setting for a prerequisite question: whether the latent state contains event-sensitive physical structure at all.

3.2 Physical Event Contexts

We use physical event context to describe the type of physical situation shown by an observed trajectory segment. An event context is not necessarily a label given to the model as input. It is a diagnostic grouping used. It helps us ask what kind of physical structure the model must represent in order to predict the sequence. In this paper, we focus on three event families: free motion, collision, and occlusion.

A free-motion context is a segment in which objects move without contact or disappearance. Prediction in this regime mainly depends on kinematic structure, such as position, velocity, and smooth motion. A collision context is a segment in which objects come into contact and their motion changes after interaction. Prediction in this regime requires sensitivity to contact, interaction, and post-contact state changes. An occlusion context is a segment in which an object becomes partially or fully hidden and later reappears. Prediction in this regime requires the model to maintain object-specific state across temporary invisibility.

These event families do not cover all of physical reasoning. They are chosen because they isolate three common demands on a physical prediction model. Free motion stresses kinematic continuation. Collision stresses interaction and contact-sensitive dynamics. Occlusion stresses object permanence. Together, they provide a controlled setting for asking whether different physical contexts reweight different latent physical structures.

Importantly, the event families are not exclusive field assignments. Collision contains kinematic approach before contact, and occlusion contains visible kinematic motion before the object is hidden. Our claim is therefore not that an event contains only one field. The claim is that the relative importance of latent physical structure should change as the event regime changes.

3.3 Latent Physical Fields

We use the term “latent physical field” to refer to a structured pattern in the hidden states of a transition model that becomes relevant under a particular class of physical states or event contexts. A field is not assumed to be a single neuron, a single coordinate, or an explicit physical variable. It may be distributed across many dimensions of the hidden state. It may also appear as a direction, subspace, cluster structure, or event-sensitive activation pattern. Our use of the term “field” is diagnostic rather than ontological. We do not assume that the model contains a human-interpretable physical module.

We focus on three latent physical fields. The kinematic field refers to hidden-state structure associated with smooth motion, position, velocity, and trajectory continuation. The contact field refers to hidden-state structure associated with object contact, collision, and post-contact change. The object-permanence field

refers to hidden-state structure associated with maintaining object identity and state across temporary invisibility.

These fields are defined by their diagnostic role, not by direct supervision. We do not train the transition model with separate field labels. We also do not require the model to expose explicit physical variables. Instead, we examine whether hidden-state patterns align with event contexts, whether field emphasis changes across event phases, and whether changing such patterns changes event-relevant predictions. A physical field is therefore a testable hypothesis about the organization of latent dynamics, not a claim that the model contains a symbolic physical module.

This definition separates our question from ordinary variable probing. A probe may show that velocity, contact, or visibility can be decoded from a hidden state. That is useful, but it mainly shows that the information is present. A latent physical field should show context sensitivity, selectivity, and functional relevance. It should not merely be readable.

3.4 State-Conditioned Field Diagnostics

We define state-conditioned field diagnostics as tests that ask whether latent physical fields become selectively relevant under different physical event contexts. The diagnostic target is not a single decoded variable. It is the relationship among three elements: the physical state or event context, the model’s hidden-state structure, and the prediction behavior of the transition model.

This distinction separates our setting from ordinary variable probing and from prediction-oriented structure learning. A standard probe may show that position, velocity, contact, or visibility can be decoded from hidden state. Other models may also use object-centric structure, kinematic variables, interaction modules, or causal factors to improve prediction, tracking, planning, or generalization. These are strong forms of physical structure. However, they do not by themselves answer a different question: how the relevance and functional role of these structures change with the physical event context.

We analyze this question at three levels. Event-level diagnostics use a sequence-level or final hidden representation to ask whether free motion, collision, and occlusion are separable and whether the corresponding field structure is emphasized. Here, an event refers to the overall physical regime of a full trajectory segment. Phase-level diagnostics operate at a finer temporal scale. We define an event phase as a diagnostic time-step label that marks where a frame lies within an event process. Free-motion sequences contain a free-motion phase. Collision sequences are divided into pre-contact, contact, and post-contact phases. Occlusion trajectories can be annotated as pre-occlusion, hidden, and reappearance phases when these phases are present within the analyzed trajectory range. Not every diagnostic necessarily uses all annotated phases; each analysis uses the phase labels that are available for the corresponding representation, prediction horizon, or time-aligned readout. These phase labels are derived from dataset annotations such as contact timing, visibility, object states, and pairwise relations. They are used only for analysis, not as model inputs. Phase-level diagnostics therefore ask how the physical demands of an event change over time. This level is a data-level proxy unless the analysis directly uses per-time-step model hidden states aligned with the same phase labels.

The three levels have different evidential strength. Event-level evidence is the main cross-architecture evidence. Phase-level proxy evidence helps interpret why collision and occlusion are mixtures rather than single-field events. Timewise hidden-state evidence is stronger, but in our current implementation it is architecture-limited. We therefore treat timewise results as supplementary evidence unless they are available

across models with comparable hidden-state interfaces.

Our goal is not to prove that the model contains explicit physical modules or human-defined physical laws. The goal is to obtain controlled evidence about how physical structure is organized, reweighted, and used inside passive transition dynamics.

4. Diagnostic Protocol

4.1 Overview

Our diagnostic protocol tests whether latent physical structure is organized and used in an event-conditioned manner. The protocol has three main parts. The first part tests separability: can hidden states distinguish free motion, collision, and occlusion? The second part tests selectivity: are event contexts associated with the expected physical field emphasis? The third part tests functional relevance: does suppressing a field-related pattern change event-relevant predictions? In the present experiments, this functional-relevance test is evaluated within the configured future prediction horizon.

We also use phase-level and timewise analyses to interpret field reweighting over event trajectories. These analyses must be read carefully. Phase-level analysis based on object states, relations, and event phases is a data-level proxy. It explains the physical structure of the event. Timewise analysis based on h_t is a hidden-state analysis. It explains how the model representation changes over time. We keep these two sources of evidence separate throughout the paper.

The protocol is a controlled diagnostic framework, not a full mechanistic explanation. Event probes may detect superficial event cues. Field selectivity may show structured association, but not functional use. Causal field effect adds intervention evidence, but still does not identify a complete mechanism. The following subsections define the components of the protocol.

4.2 Event Probe

The first part of the protocol asks whether the model's hidden states separate different physical events. Given a hidden state h_t , we train a lightweight probe to classify whether the sequence is free motion, collision, or occlusion. The event label is used only for diagnosis. It is not given to the transition model as an input.

This probe answers a basic question: does the hidden state contain information about which physical situation the model is currently predicting? A successful event probe does not prove that the model has learned a kinematic field, a contact field, or an object-permanence field. It only shows that event-regime information is readable from the hidden representation.

4.3 Field Selectivity

The second part of the protocol asks whether event contexts are associated with the expected field emphasis. We do not interpret the mapping as one-to-one or exclusive. Instead, field selectivity measures relative emphasis. Free motion should be kinematic-dominant. Collision should retain kinematic structure but place additional emphasis on contact-sensitive structure. Occlusion should retain motion-related structure but place additional emphasis on object-permanence structure during hidden or reappearance phases.

Field selectivity compares field-related hidden-state patterns across event types and controls. A field is selective if it is stronger, more diagnostic, or more useful in the event type where it is expected. This part goes beyond ordinary variable probing because it asks whether the model emphasizes the relevant physical

structure under the event condition where that structure matters.

4.4 Causal Field Effect (CFE)

The third part of the protocol asks whether a field-related pattern matters for prediction. We call this causal field effect. If a hidden-state pattern is important for a physical event, then changing or suppressing that pattern should affect the model’s prediction for that event. In the present implementation, CFE is measured as a prediction-loss change inside event-relevant windows that fall within the configured fixed future horizon. For example, if a contact field is functionally relevant, suppressing a contact-related pattern should affect collision predictions more than free-motion predictions. If an object-permanence field is functionally relevant, suppressing an object-permanence-related pattern should affect hard-occlusion predictions. We interpret causal field effect as evidence of causal sensitivity, not as a full explanation of the model’s mechanism. To avoid over-interpreting the intervention, we compare target-field suppression with controls such as random subspaces, matched-norm random directions, mismatched fields, and field-label shuffles.

4.5 Controls and Input Variants

The protocol includes controls for shortcut and leakage. If the model receives direct event labels, contact labels, future states, or hidden true states as input, then a probe or field diagnostic may succeed for trivial reasons. We therefore test whether the diagnostic signals persist after removing obvious shortcut information from the input. First, we use a motion-only setting in which the model receives only object-level position and velocity, without explicit event, contact, or occlusion labels. Second, for occlusion sequences, we use an observation-like setting in which the model receives only visible state information and visibility indicators, without access to the true hidden state of the occluded object. If the diagnostic signals remain under these restricted settings, they are less likely to be explained by direct label leakage or trivial input cues.

5. Dataset and Models

5.1 Main Controlled Public-Generator Dataset

Our main experiments use a Kubric-style public-generator pipeline to construct an object-state dataset (Greff et al., 2022). The dataset is designed for diagnostic analysis, not as a general-purpose video benchmark. In our dataset, physical event types are balanced, object-level states are available, and diagnostic labels can be separated from model inputs.

The main dataset contains three event families: free motion, collision, and occlusion. Each family contains 300 sequences, giving 900 sequences in total. Free-motion sequences test kinematic continuation. Collision sequences test contact-sensitive interaction. Occlusion sequences test object permanence when an object becomes temporarily hidden. This balanced design lets us compare event-conditioned latent structure across physical regimes without making the analysis dominated by a single event type.

The dataset provides object-level information and diagnostic annotations. These include object states, masks, centroid heatmaps, pairwise relations, event family labels, event phase labels, and metadata. Collision sequences are audited to ensure that they contain true contact events, rather than only near-contact cases. Occlusion sequences are divided into easy and hard cases.

The dataset also contains held-out stress-test splits. For collision, the held-out split emphasizes more difficult collision regimes, such as larger collision angles and higher approach-speed conditions. For occlusion, the

held-out split emphasizes longer hard-occlusion windows. We refer to these as out-of-distribution, or OOD, tests, which means testing on harder parameter regimes within the same controlled generator setting.

5.2 Event Families and Annotations

The dataset contains three event families: free motion, collision, and occlusion. These event families are not meant to cover all possible physical situations. They are chosen because they place different demands on a passive object-state prediction model.

In free-motion sequences, objects move without contact and without becoming hidden. In collision sequences, two or more objects come into contact and their motion changes after interaction. In occlusion sequences, an object becomes partially or fully hidden and later reappears. The dataset also records event phases such as pre-contact, contact, post-contact, pre-occlusion, hidden, and reappearance. These phase labels are used for analysis and auditing. They are not treated as ordinary model inputs.

This annotation design allows us to compare free motion, collision, and occlusion under a shared object-state format. It also allows us to distinguish event-level diagnostics from phase-level proxy analysis.

5.3 Transition Models

We evaluate the diagnostic protocol on three passive object-state transition models: a GRU-based recurrent model, a Transformer-lite model, and an RSSM-lite model. These models serve as architecture-family controls. The purpose is to test whether the diagnostic results depend on one particular transition architecture, or whether similar event-conditioned patterns can be observed across different ways of modeling temporal dynamics.

The GRU-based model represents a recurrent transition architecture. The Transformer-lite model represents an attention-based transition architecture. The RSSM-lite model represents a latent state-space style transition architecture. We do not claim that the RSSM-lite variant is equivalent to a full Dreamer-style agent. We use it only to test whether the diagnostic protocol remains meaningful in a state-space transition setting. For all three models, the diagnostic target is the hidden representation produced during passive prediction. We train the models to predict future object states. We then analyze their hidden states using event probes, field selectivity, causal field effect, and timewise readouts when appropriate.

5.4 Input Variants and Leakage Control

We evaluate several input variants. The first variant uses object-state information for passive prediction. The second variant is a kinematic-only input, which uses only basic motion variables such as object position and velocity. The third variant is an observation-like input, which is designed for occlusion. It uses visible state information, the last observed position, and a visibility flag, without giving the model the true hidden position of an occluded object.

A central risk in event-conditioned diagnostics is shortcut learning. If the model directly receives event labels, contact labels, future states, or hidden true states as input, then the diagnostic may succeed for a trivial reason. To avoid this problem, event family labels, event phase labels, contact labels, future states, and hidden true object states are absent from context inputs. They are used only to define diagnostic groups, check dataset quality, and compute evaluation metrics.

5.5 Training and Diagnostic Readouts

All transition models are trained for passive future-state prediction. Given an observed prefix of object states, the model predicts future object states. The training objective is prediction loss on future object states. The models are trained separately for each architecture, input variant, and random seed. The main evaluation uses the in-distribution test split. Held-out collision and occlusion splits are used later for stress tests. In the reported experiments, the primary training and evaluation interface is fixed-horizon: an observed prefix is used to predict a configured future horizon.

After training, we analyze the hidden states of the trained transition models. The diagnostic readouts are fitted after the transition model has learned the prediction task. They are used only for analysis, not used to train the transition model, and their labels are not given to the model as input.

The first readout is an event probe. Both standard variable probes and our event probe take model hidden states as input. The difference lies in the prediction target. A standard variable probe usually predicts a specific physical variable, such as position, velocity, contact, or visibility; while our event probe predicts the physical event regime of the sequence: free motion, collision, or occlusion.

Field selectivity and causal field effect ask stronger questions. Field selectivity tests whether hidden-state patterns align with expected field emphasis. CFE tests whether suppressing a field-related pattern changes event-relevant predictions. Exact architecture sizes, optimizer settings, training epochs, normalization details, and intervention implementation are provided in Appendix A.

6. Main results

6.1 Models Learn Predictive Dynamics and Encode Event-Regime Information

Before analyzing latent physical fields, we first check whether the models have learned the basic predictive dynamics of the dataset. Table 1 reports this check under the kinematic-only input setting. Here, kinematic-only refers to the input variant, not to the free-motion event family. Across all evaluated architectures and seeds, the learned models predict future object states better than the constant-velocity baseline in the in-distribution test split. This result shows that the transition models have learned useful object-state dynamics, rather than producing arbitrary hidden states. It also gives a basic foundation for later latent-state diagnostics.

We then apply the event probe defined in Section 4.2. Prior work has already shown that physical variables can often be decoded from learned representations. Here, the probe mainly checks whether, in our trained passive object-state models, the hidden states contain stable information about the current event regime.

As shown in Table 1, the event probe succeeds across the evaluated models and seeds. This result shows that event-regime information is available in the hidden states. We do not interpret event-probe success as evidence of a physical field by itself. The main evidence comes from whether the event-related structure aligns with field emphasis, whether it changes over event phases, and whether suppressing a field-related pattern changes event-relevant predictions.

Table 1 Prediction sanity and event-regime readout under kinematic-only input. Seed denotes the random seed used for model training and evaluation. MSE denotes normalized future-position MSE over predicted object x/y coordinates in the fixed-horizon target window. CV_MSE is the same metric computed for the constant-velocity baseline. Event probe F1 is the macro-F1 score of the lightweight probe that predicts free

motion, collision, or occlusion from frozen model hidden states.

Model	Seed	MSE	CV_MSE	MSE/CV	Probe F1	Verdict
GRU	3407	2.46E-04	3.35E-04	0.73	1.00	Pass
Transformer	3407	9.98E-05	3.35E-04	0.30	1.00	Pass
RSSM	3407	1.49E-04	3.35E-04	0.45	1.00	Pass
GRU	3408	2.23E-04	3.35E-04	0.66	1.00	Pass
Transformer	3408	1.21E-04	3.35E-04	0.36	1.00	Pass
RSSM	3408	1.40E-04	3.35E-04	0.42	1.00	Pass

6.2 Event Contexts Reweight Non-Exclusive Physical Fields

The event probe in Section 6.1 shows that the hidden states contain information about the current physical event. We now ask a stronger question: how is this event information organized with respect to the physical fields defined in Section 3.3? Our results do not imply a one-to-one mapping between events and exclusive fields. Rather, different event contexts systematically shift the relative weighting among multiple physical fields.

A collision sequence is not purely a contact process. Before contact, it still contains ordinary motion and approach dynamics. An occlusion sequence is not purely an object-permanence process either. Before the object becomes hidden, it still contains visible motion, and after reappearance it again contains visible-state information. For this reason, we interpret field selectivity as relative field emphasis, not as a one-to-one event-to-field assignment. In our setting, free motion is expected to be mainly kinematic-dominant; collision is expected to combine kinematic and contact structure; and occlusion is expected to combine kinematic and object-permanence structure.

Figure 1 presents the results of physical-field reweighting induced by event contexts at event, phase, and timewise levels. Event-level diagnostics use a sequence-level hidden representation to ask whether free motion, collision, and occlusion differ in their relative field emphasis. Phase-level diagnostics use dataset-defined event phases to describe how the physical demands of a trajectory change over time. For collision, we divide the sequence into pre-contact, contact, and post-contact phases. For occlusion, we divide the sequence into pre-occlusion and hidden phases, and include reappearance when that phase is available in the selected analysis. These phase-level results are data-level proxies unless they are computed from per-time-step hidden states. Finally, timewise diagnostics use per-time-step hidden states, when available, to test whether field scores shift over event phases inside the learned representation.

For figures concerning the hidden-state, i.e. Figure 1A, D, and E, the y-axis reports a field readout score: a softmax probability produced by a trained 3-class linear probe applied to z-scored hidden states. For Figure 1B and C, the y-axis reports a data-level proxy z-score computed from annotated object-state and event-phase information, not a model activation. For Figure 1F, the y-axis reports a positive shift fraction rather than a readout magnitude. Appendix B gives the mathematical definitions and aggregation rules for these quantities.

At the event level, the RSSM hidden-state readouts support the expected ordering of field emphasis. Figure 1A shows that free motion is strongly kinematic-dominant. Collision retains a substantial kinematic component, but also shows a clear rise in the contact field. Occlusion retains a residual motion-related component, but shows a much stronger object-permanence field. This is the main cross-event result. It shows that the representation does not simply store generic trajectory information. Instead, the relative weighting

of physical structure changes systematically with event context.

We then use phase-level proxy analysis to interpret why collision and occlusion should be viewed as mixed events rather than single-field events. This analysis uses object states, pairwise relations, and event-phase labels from the dataset. It does not use model hidden states. Its role is to describe the changing physical demands of the trajectory itself. In the collision case, Figure 1B shows a transition from kinematic-dominant pre-contact motion to contact-sensitive interaction at the contact phase, followed by a partial return to a more kinematic regime after contact. In the occlusion case, Figure 1C shows a transition from visible kinematic motion before hiding to object-permanence-dominant structure during the hidden interval. When reappearance is included, visible-state structure partially returns, but object-permanence remains elevated relative to pre-occlusion. These proxy profiles explain why event-conditioned field diagnostics should not be interpreted as hard category boundaries.

The next question is whether a similar reweighting pattern appears inside model hidden states over time. For RSSM future rollout latents, the answer is yes. Figure 1D and E show time-aligned hidden-state field dynamics. In collision sequences aligned to contact onset, kinematic scores are higher before contact, while contact scores rise around the event boundary and dominate afterward. In occlusion sequences aligned to hidden-start, kinematic scores are higher before hiding, while object-permanence scores rise sharply around the hidden interval and remain dominant afterward. A strict phase-aware field readout on RSSM hidden states reaches a mean test macro-F1 of 0.900, which provides direct time-resolved evidence that field structure changes with event phase inside the learned representation.

For GRU and Transformer-lite, we do not claim the same level of time-resolved evidence as in RSSM rollout latents, because the current implementations expose sequence-level or prefix-conditioned hidden representations rather than a directly comparable future rollout latent trajectory. Instead, we use a lighter sliding-prefix hidden-state analysis. This analysis tests whether the direction of the expected field shift is present as prefixes move across event phases, but it does not reconstruct full phase-resolved hidden dynamics within a single future rollout. Across the evaluated cases, contact-related scores increase at collision phases, and object-permanence-related scores increase at hidden phases. The joint directional consistency score is 1.000, with positive contact-phase and hidden-phase shifts in all evaluated GRU and Transformer-lite cases. Figure 1F summarizes this weaker but still consistent evidence.

Taken together, the results support a hierarchical interpretation. First, at the event level, hidden states separate physical regimes and show different relative field emphasis. Second, phase-level proxy analysis explains why collision and occlusion are mixtures rather than single-field events. Third, timewise hidden-state analysis shows phase-aligned field reweighting inside model representations, strongest in RSSM rollout latents and directionally consistent in GRU and Transformer-lite. This is stronger than ordinary variable probing, because it studies how field emphasis changes with event context and event phase. At the same time, we do not claim a full mechanistic decomposition. Our evidence supports event-conditioned field reweighting in passive object-state world models, not the discovery of explicit field modules.

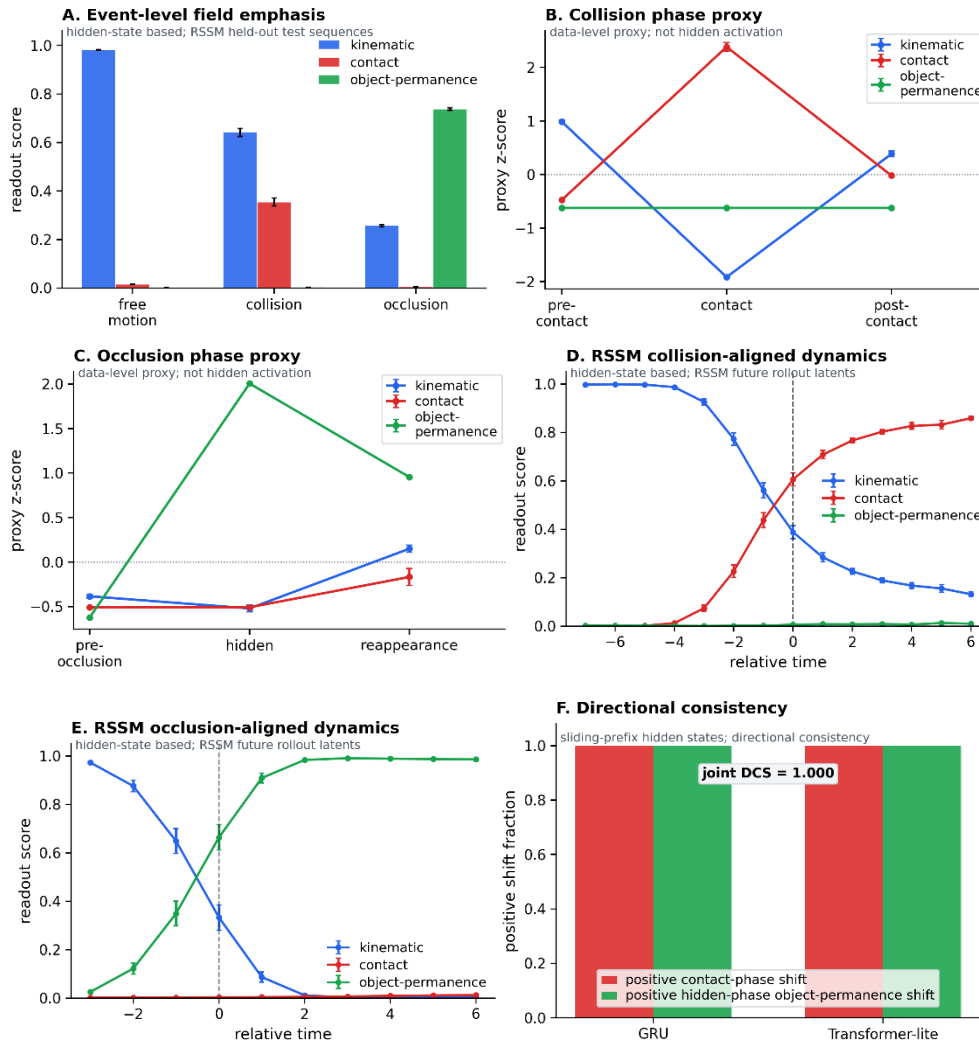


Figure 1 Event contexts reweight non-exclusive physical fields at event, phase, and timewise levels. The panels use different y-axes because they report different diagnostics: Panels A, D, and E report softmax probabilities from a 3-class linear probe applied to z-scored hidden states; Panels B and C report data-level proxy z-scores computed from annotated object-state and event-phase information; and Panel F reports the fraction of evaluated GRU and Transformer-lite cases with positive shifts in the expected field direction. Values should therefore be compared within each panel rather than across panels. (A) Event-level hidden-state field readouts on RSSM test sequences. Free motion is strongly kinematic-dominant; collision combines a substantial kinematic component with increased contact emphasis; occlusion combines a residual kinematic component with much stronger object-permanence emphasis. (B-C) Phase-level proxy profiles computed from annotated data-level structure rather than hidden activations. In collision, the proxy pattern shifts from kinematic-dominant pre-contact motion to contact-sensitive interaction at contact, followed by a partial return toward a more kinematic regime post-contact. In occlusion, the proxy pattern shifts from visible-motion structure before hiding to object-permanence-dominant structure during the hidden interval; when reappearance is included, visible-state structure partially returns while object-permanence remains elevated. (D-E) Time-aligned RSSM future-rollout latent readouts show analogous hidden-state reweighting around contact onset (D) and hidden-start (E): kinematic scores decrease while contact or object-permanence scores increase and become dominant. (F) A lighter sliding-prefix hidden-state analysis for GRU and Transformer-lite provides weaker but consistent directional evidence: contact-related scores increase at collision phases and object-permanence-related scores increase at hidden phases in all evaluated cases,

yielding a joint directional consistency score (DCS) of 1.000. Overall, the figure supports event-conditioned field reweighting rather than exclusive event-to-field assignment or explicit field modules.

6.3 Fixed-horizon Windowed Projection CFE

Sections 6.1 and 6.2 show that event-regime information is readable from hidden states and that event contexts reweight non-exclusive physical field readouts. These results establish representational organization, but readout evidence alone does not show whether the corresponding representational structure matters for prediction. We therefore ask a further question: if a field-aligned component of the hidden representation is suppressed, does prediction degrade in the event regime where that field is expected to matter?

We answer this question with CFE. In the present fixed-horizon setting, CFE is defined as the increase in normalized x/y position prediction loss after a field-aligned projection intervention. The intervention is evaluated on event-relevant frame windows that fall within the configured future prediction horizon. This restriction follows from the forecasting setup: the model observes the first eight frames and predicts the next eight frames, so CFE can only be computed on frames for which both the base model and the perturbed model produce predictions. Appendix C gives the mathematical definitions, field-direction construction, normalization procedure, intervention operator, controls, and aggregation rules.

Figure 2A summarizes the fixed-horizon event-window coverage for the collision-contact and hard-occlusion hidden-window analyses. The reinforced CFE analysis uses trained checkpoints and does not retrain the world models. The intervention suppresses a probe-derived field direction in the normalized hidden-state space and then decodes the perturbed representation to measure the resulting prediction-loss increase. For GRU and Transformer-lite, the perturbed representation is decoded through the corresponding prediction head. For RSSM-lite, the reported result is a head-decoding CFE from the perturbed latent state, not a full RSSM transition re-rollout. We therefore interpret the results as fixed-horizon functional sensitivity at the representational-subspace level, not as evidence of explicit physical modules or complete rollout-level causal mechanisms.

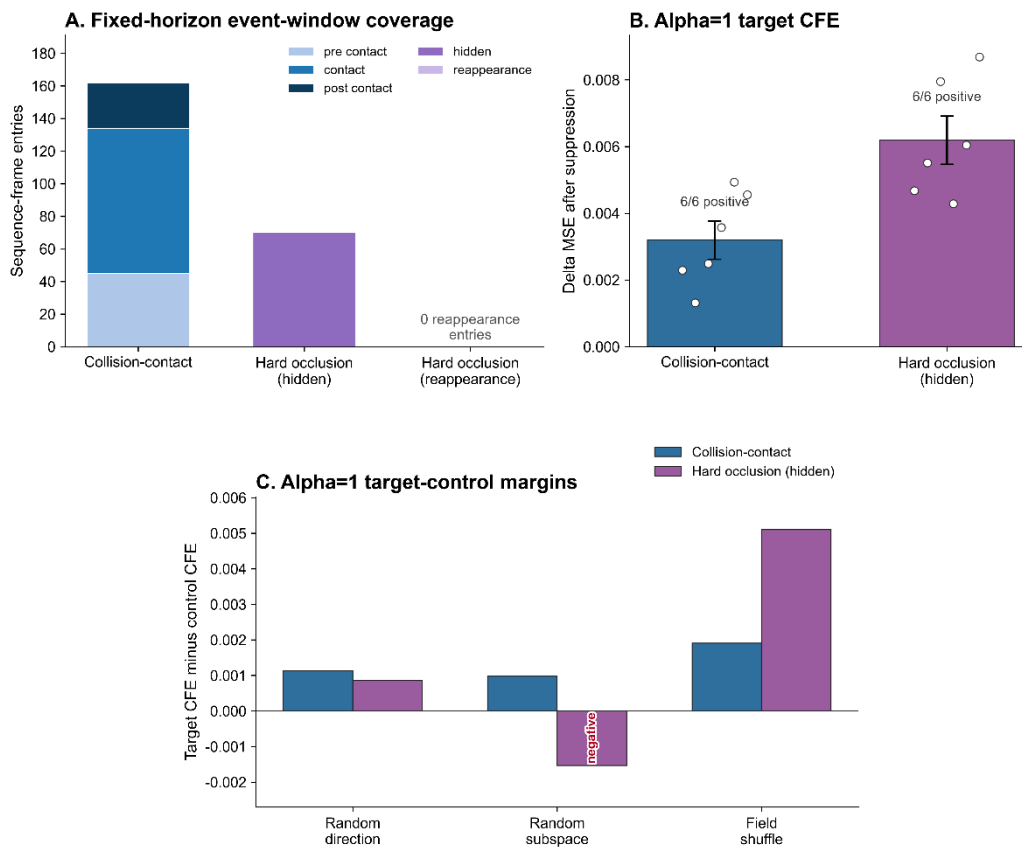
Figure 2B shows that the collision-contact result has the clearest functional-sensitivity evidence. Suppressing the contact-aligned projection increases collision-window prediction loss in all evaluated architecture-seed cases at full suppression strength. The mean target CFE for collision-contact is 0.00319 in normalized x/y prediction-loss units, with 6/6 positive cases. The effect also remains positive relative to all reported controls at the mean level: the target-minus-random margin is 0.00113, the target-minus-random-subspace margin is 0.00098, the target-minus-field-shuffle margin is 0.00190, as shown in Figure 2C. In addition, Figure 2D shows that all six evaluated cases show a positive dose trend across suppression strengths. Together, these results indicate that contact-aligned representational structure is functionally relevant to collision-window prediction in the fixed-horizon forecasting task.

The hard-occlusion hidden-window result is positive but less specific. Suppressing the object-permanence-aligned projection increases hidden-window prediction loss in all evaluated architecture-seed cases at full suppression strength. The mean target CFE for hard occlusion is 0.00619, with 6/6 positive cases and positive dose trends in all evaluated cases, as shown in Figure 2B and Figure 2D. However, the control margins are mixed. As shown in Figure 2C, the target-minus-random margin is positive (0.00086), the target-minus-field-shuffle margin is positive (0.00510), but the target-minus-random-subspace margin is negative (-0.00153). We therefore interpret the hard-occlusion result as evidence of hidden-window functional sensitivity, with weaker subspace-specificity than the collision result. It supports the relevance of object-permanence-aligned

structure during hidden intervals, but it should not be read as isolating a unique object-permanence mechanism.

These CFE results strengthen the interpretation of the readout results in Section 6.2. The hidden states do not merely contain event-regime information that can be decoded by a probe. When field-aligned components are suppressed, predictions in the corresponding event-relevant windows become worse, especially for collision-contact. This provides functional-sensitivity evidence beyond ordinary probing. However, the projection-suppression tests do not establish that the model contains explicit physical modules, isolated causal circuits, or a complete mechanistic decomposition.

Taken together, the results support a fixed-horizon functional-relevance claim: in passive object-state world models, event-conditioned field-aligned representational structure has predictive consequences in the event regimes where it is expected to matter. The evidence is strongest for contact-aligned structure in collision-contact windows and positive but more qualified for object-permanence-aligned structure in hard-occlusion hidden windows.



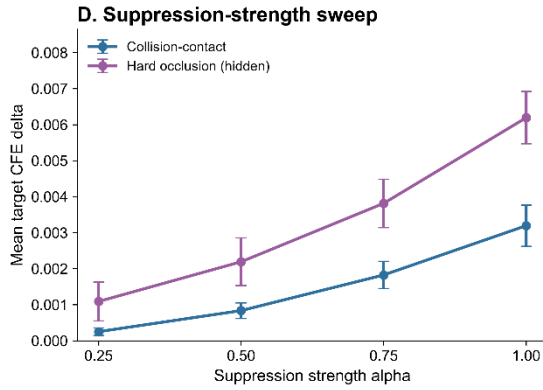


Figure 2 Windowed projection CFE supports fixed-horizon functional sensitivity. (A) Event-window coverage used for CFE. Collision-contact windows include pre-contact, contact, and post-contact entries within the configured future horizon; hard-occlusion windows include hidden entries only, with no reappearance entries in the fixed-horizon CFE analysis. (B) Mean target CFE at full suppression strength ($\alpha = 1$) for collision-contact and hard-occlusion hidden windows. Points indicate architecture-seed cases where available. (C) Target-control margins at $\alpha = 1$. Collision-contact has positive mean margins against all reported controls, whereas hard occlusion has positive margins against random and field-shuffle controls but a negative margin against the random-subspace control. (D) Suppression-strength sweep showing dose trends for target CFE and controls. The figure supports fixed-horizon functional sensitivity rather than explicit physical modules or full rollout-level causal mechanisms.

6.4 Summary of experiment results

The results above support a hierarchical interpretation of event-conditioned latent physical structure in passive object-state world models. Section 6.1 establishes that the trained transition models learn useful fixed-horizon predictive dynamics and that event-regime information is readable from their hidden states. Section 6.2 shows that this event information is not only separable, but also organized as a reweighting of non-exclusive physical field readouts. Section 6.3 further illustrates that suppressing field-aligned representational components can affect event-relevant prediction, providing fixed-horizon functional-sensitivity evidence beyond ordinary probing.

In our experiments, collision sequences retained kinematic structure while increasing contact emphasis, and occlusion sequences retained motion-related structure while increasing object-permanence emphasis. These results imply event-conditioned reweighting of multiple overlapping physical fields. This finding is consistent with the non-exclusive field view introduced in Section 3.3: physical fields are diagnostic patterns in hidden-state organization, not isolated symbolic modules.

The functional evidence is strongest for contact-aligned structure in collision-contact windows. Contact-aligned projection suppression increases prediction loss in the corresponding fixed-horizon event window and shows positive margins against the main same-window controls. For hard occlusion, object-permanence-aligned suppression produces positive hidden-window CFE, but the result is more qualified. It supports functional sensitivity during hidden intervals, but it is not reappearance-window evidence or as isolation of a unique object-permanence mechanism. In other words, the evidence supports fixed-horizon functional sensitivity at the representational-subspace level. But it does not establish explicit physical modules, isolated causal circuits, full RSSM transition re-rollout effects, or complete mechanistic decomposition.

Taken together, Sections 6.1–6.3 support the following bounded conclusion: in a controlled fixed-horizon

passive forecasting setting, event contexts systematically shape latent physical-field emphasis, and field-aligned representational components have predictive consequences in the event regimes where they are expected to matter. The main contribution is a controlled diagnostic protocol for testing event-conditioned latent physical structure in passive object-state prediction. The protocol does not claim to identify complete mechanisms, but it offers a reusable diagnostic template for probing, comparing, and stress-testing latent physical representations in other predictive models.

7. Discussion and Limitations

7.1 Contribution of our diagnostic protocol

The central contribution of this work is not a new transition architecture or a new physical prediction benchmark, but a diagnostic protocol for asking how latent physical structure is organized and used under different event contexts. Standard prediction metrics tell us whether a model predicts well. Standard probes tell us whether a variable or event label is decodable. Our protocol adds a different layer of analysis: it asks whether event contexts reweight non-exclusive physical field readouts, and whether field-aligned representational structure has measurable consequences for prediction.

This distinction is important because physical information can be present in a hidden state without being organized or used in an event-sensitive way. A model may encode position or velocity but still fail to use contact-sensitive structure during collision, or maintain visible trajectory information without using object-permanence-related structure during occlusion. By combining event probes, field readouts, phase-level proxies, time-aligned readouts, and fixed-horizon projection CFE, the protocol provides a controlled way to separate readability, event-conditioned organization, and functional sensitivity.

The protocol is intentionally diagnostic rather than architectural. It can be applied to recurrent, attention-based, or state-space transition models without requiring those models to expose explicit physical variables or modules. This makes it useful as a comparative tool: different models can be evaluated not only by their prediction loss, but also by how their hidden states organize and use physical field structure under matched event conditions.

7.2 Scope and limitations

The main limitation is the controlled fixed-horizon setting. In the reported experiments, models observe the first eight frames and predict the next eight frames. This design makes cross-architecture comparisons more interpretable, because all models receive the same observed prefix and are evaluated over the same future horizon. However, it does not establish arbitrary sliding-context generalization. A model that exhibits event-conditioned structure under this fixed forecasting interface may behave differently under event-aligned sliding windows, longer horizons, or online rollout.

A second limitation is the use of object-state inputs rather than raw video. This choice removes the confound of object discovery and visual perception, allowing the analysis to focus on transition dynamics. It also means that the results should not be interpreted as evidence that raw-video world models automatically discover the same fields. Extending the protocol to raw pixels would require stable object extraction, segmentation, or learned object-centric representations.

A third limitation concerns the CFE intervention. Projection suppression targets a readout-aligned representational direction, not an explicit module. A positive CFE indicates functional sensitivity of a representational subspace under the configured prediction setting. It does not prove that the model contains

a discrete contact module, object-permanence module, or isolated causal circuit. For RSSM-lite, the reported CFE is a head-decoding sensitivity test from a perturbed latent state, not a full transition re-rollout intervention. The hard-occlusion CFE result is also limited to hidden-window prediction; the current fixed-horizon analysis does not support a reappearance-window CFE claim. These boundaries are important for interpreting the functional evidence conservatively.

The event taxonomy is also limited. Free motion, collision, and occlusion isolate three important physical demands: kinematic continuation, contact-sensitive interaction, and object permanence. They do not cover support, containment, gravity, rolling, stacking, fluid dynamics, deformable objects, multi-body interactions, or action-conditioned physical change. The field vocabulary should therefore be viewed as a minimal diagnostic basis, not a complete taxonomy of physical understanding.

7.3 Future extensions

Several extensions follow naturally. First, the fixed-horizon protocol can be extended to sliding-context or longer-horizon forecasting, but this requires models trained or adapted to that evaluation regime. Second, future work can implement full rollout interventions for recurrent state-space models, so that perturbations propagate through the transition dynamics rather than only through a prediction head. Third, the diagnostic field set can be expanded beyond kinematics, contact, and object permanence to include support, containment, gravity, stability, friction, and action-conditioned affordances.

A broader direction is to apply the protocol to raw-video world models and action-conditioned agents. In such settings, the diagnostic question becomes whether visual perception, object discovery, control, and latent physical structure interact in event-conditioned ways. The controlled object-state setting studied here should be viewed as a first step: it isolates the transition-dynamics question before adding the additional complexity of perception and action.

8. Conclusion

We introduced a controlled diagnostic protocol for testing event-conditioned latent physical structure in passive object-state world models. Rather than asking only whether a model predicts future states or whether physical variables are decodable, the protocol asks whether event contexts organize, reweight, and functionally recruit non-exclusive physical field structure.

In a balanced controlled-generator dataset with free-motion, collision, and occlusion events, we showed that trained transition models learn useful fixed-horizon predictive dynamics, encode event-regime information in their hidden states, and exhibit event-conditioned reweighting of kinematic, contact, and object-permanence field readouts. Fixed-horizon projection CFE further shows that suppressing field-aligned representational components can affect event-relevant prediction, with the strongest evidence for contact-aligned structure in collision-contact windows and more qualified evidence for object-permanence-aligned structure in hard-occlusion hidden windows. This work provides a reusable diagnostic template for probing, comparing, and stress-testing latent physical representations in other predictive models and controlled world-model settings.

References

- Alam, N. (2026). Causal Physics Steering in Video World Models via Concept Activation Vectors. Proceedings of the IEEE/CVF Conference on Computer Vision and Pattern Recognition,
- Bakhtin, A., van der Maaten, L., Johnson, J., Gustafson, L., & Girshick, R. (2019). Phyre: A new benchmark for physical reasoning. *Advances in Neural Information Processing Systems*, 32.
- Bear, D. M., Wang, E., Mrowca, D., Binder, F. J., Tung, H.-Y. F., Pramod, R., Holdaway, C., Tao, S., Smith, K., & Sun, F.-Y. (2021). Physion: Evaluating physical prediction from vision in humans and machines. *arXiv preprint arXiv:2106.08261*.
- Bordes, F., Garrido, Q., Kao, J. T., Williams, A., Rabbat, M., & Dupoux, E. (2025). Intphys 2: Benchmarking intuitive physics understanding in complex synthetic environments. *arXiv preprint arXiv:2506.09849*.
- Ding, Z., Lai, X., Chen, W., Zhang, X.-P., & Chen, J. (2026). CausalVAE as a Plug-in for World Models: Towards Reliable Counterfactual Dynamics. *arXiv preprint arXiv:2604.07712*.
- Girdhar, R., & Ramanan, D. (2019). Cater: A diagnostic dataset for compositional actions and temporal reasoning. *arXiv preprint arXiv:1910.04744*.
- Greff, K., Belletti, F., Beyer, L., Doersch, C., Du, Y., Duckworth, D., Fleet, D. J., Gnanaprasam, D., Golemo, F., & Herrmann, C. (2022). Kubric: A scalable dataset generator. Proceedings of the IEEE/CVF conference on computer vision and pattern recognition,
- Ha, D., & Schmidhuber, J. (2018). World models. *arXiv preprint arXiv:1803.10122*, 2(3), 440.
- Hafner, D., Lillicrap, T., Fischer, I., Villegas, R., Ha, D., Lee, H., & Davidson, J. (2019). Learning latent dynamics for planning from pixels. International conference on machine learning,
- Hafner, D., Pasukonis, J., Ba, J., & Lillicrap, T. (2023). Mastering diverse domains through world models. *arXiv preprint arXiv:2301.04104*.
- Joseph, S., Garrido, Q., Balestriero, R., Kowal, M., Fel, T., Bakhtiari, S., Richards, B., & Rabbat, M. (2026). Interpreting physics in video world models. *arXiv preprint arXiv:2602.07050*.
- Lei, A., Schölkopf, B., & Posner, I. (2022). Variational causal dynamics: Discovering modular world models from interventions. *arXiv preprint arXiv:2206.11131*.
- Micheli, V., Alonso, E., & Fleuret, F. (2022). Transformers are sample-efficient world models. *arXiv preprint arXiv:2209.00588*.
- Röder, F., Benad, J., Eppe, M., & Banerjee, P. (2026). Dynamics-aligned latent imagination in contextual world models for zero-shot generalization. *Advances in Neural Information Processing Systems*, 38, 72736–72771.
- Shamsian, A., Kleinfeld, O., Globerson, A., & Chechik, G. (2020). Learning object permanence from video. European Conference on Computer Vision,
- Song, Y.-J., Kim, J., Choi, S., Kim, J.-H., & Zhang, B.-T. (2025). OCK: Unsupervised Dynamic Video Prediction with Object-Centric Kinematics. Proceedings of the IEEE/CVF International Conference on Computer Vision,
- Traub, M., Becker, F., Otte, S., & Butz, M. V. (2024). Learning object permanence from videos via latent imaginations. International Conference on Artificial Neural Networks,

- Villar-Corrales, A., Wahdan, I., & Behnke, S. (2023). Object-centric video prediction via decoupling of object dynamics and interactions. 2023 IEEE International Conference on Image Processing (ICIP),
- Wu, Z., Dvornik, N., Greff, K., Kipf, T., & Garg, A. (2022). Slotformer: Unsupervised visual dynamics simulation with object-centric models. *arXiv preprint arXiv:2210.05861*.
- Yi, K., Gan, C., Li, Y., Kohli, P., Wu, J., Torralba, A., & Tenenbaum, J. B. (2019). Clevrer: Collision events for video representation and reasoning. *arXiv preprint arXiv:1910.01442*.
- Zhang, X. (2026). What Do World Models Learn in RL? Probing Latent Representations in Learned Environment Simulators. *arXiv preprint arXiv:2603.21546*.

Appendix A. Experimental and Diagnostic Details

This appendix documents the fixed-horizon scale/OOD evaluation used as the methodological baseline for the manuscript. The goal is to make the controlled public-generator experiment, model training, hidden-state extraction, event probing and Causal Field Effect (CFE) audit history reproducible. The original baseline CFE sweep documented here is retained as baseline and audit information; the primary fixed-horizon windowed projection CFE results reported in Section 6.3 and Figure 2 are defined separately in Appendix C.

A.1 Dataset generation

The fixed-horizon scale/OOD evaluation generated the controlled robustness dataset `physem_publicgen_balanced_v2_scale_ood`. The dataset contains three event families: free motion, collision, and occlusion. Each event family contains 300 sequences, for a total of 900 sequences. Each sequence has 30 frames, two object slots, 64×64 rendered frames, object masks, centroid heatmaps, pairwise relation tensors, event-family labels, event-phase labels, sequence identifiers, and metadata.

Item	Value
<code>experiment_id</code>	<code>fixed_horizon_scale_ood_evaluation_v0</code>
<code>dataset</code>	<code>physem_publicgen_balanced_v2_scale_ood</code>
<code>n_sequences</code>	900
<code>n_per_event</code>	300
<code>events</code>	<code>free_motion, collision, occlusion</code>
<code>sequence_length_T</code>	30
<code>resolution</code>	64×64
<code>objects_K</code>	2
<code>context_length</code>	8
<code>future_horizon</code>	8
<code>dataset_seed</code>	7707

The object-state fields are: `x`, `y`, `vx`, `vy`, `visible`, `occluded`, `object_id`, `radius`, `mass`, `shape_id`. The pairwise-relation fields are: `distance`, `near_contact`, `contact`, `relative_vx`, `relative_vy`, `collision_phase`. The stored tensor set is: `frames`, `object_states`, `object_masks`, `centroid_heatmaps`, `pairwise_relations`, `event_family`, `event_phase`, `metadata_json`.

Collision sequences were generated with true-contact dynamics rather than near-contact-only templates. The dataset audit reports a collision true-contact rate of 1.000 and a mean contact-frame count of 1.513. Occlusion sequences are balanced into 150 easy-occlusion and 150 hard-occlusion sequences.

The fixed-horizon scale/OOD evaluation split structure is:

Split	Count
train	590
val	126
test	127
test_id	127
test_ood_collision	45
test_ood_occlusion	12

The OOD split is a controlled-generator parameter split, not a real-video transfer split. Collision OOD uses held-out high-angle/high-speed regimes; occlusion OOD uses longer hard-occlusion windows.

OOD item	Value
split_id	scale_ood_v0
collision rule	top 15 percent by collision_angle_abs plus high approach speed
occlusion rule	hidden_duration >= 11 and hard occlusion
collision angle train mean	2.4423
collision angle OOD mean	12.8934
collision approach speed train mean	2.4176
collision approach speed OOD mean	2.4625
hidden duration train mean	8.0644
hidden duration OOD mean	12.0000
split overlap found	False

A.2 Model training

The fixed-horizon scale/OOD evaluation trains three passive object-state transition architecture families: GRU-R2h-loss-long, Transformer-lite full-pass configuration, and RSSM-large-position-heavy-long. These are architecture-family controls rather than new model contributions. Each architecture is trained with two random seeds, 3407 and 3408, under two input variants: `kinematic_only` and `observation_like`.

The `kinematic_only` variant uses normalized $x/y/v_x/v_y$ fields from the context window. The `observation_like` variant uses visible x/y , last observed x/y , and a visibility flag; hidden true object state is not provided as an input. Event labels, event phases, contact labels, pairwise relations, and future targets are not used as model context inputs.

Training item	Fixed-horizon value
architectures	GRU-R2h-loss-long; Transformer-lite full-pass configuration; RSSM-large-position-heavy-long
input variants	kinematic_only, observation_like
seeds	3407, 3408
optimizer	AdamW
learning rate	0.001
weight decay	0.0001
batch size	96
max epochs	120
early stopping patience	24
LR scheduler	ReduceLROnPlateau(mode='min', patience=12, factor=0.55)
gradient clipping	global norm clipped to 1.0
loss weights	position=1.0, velocity=0.2, visibility=0.05, occlusion=0.05
evaluation batch size	128
device	cuda if available else cpu

The training objective is a weighted MSE over predicted future object state fields. The implemented loss is:

$$\text{loss} = 1.0 \times \text{position_mse} + 0.2 \times \text{velocity_mse} + 0.05 \times \text{visibility_mse} + 0.05 \times \text{occlusion_mse}.$$

For every run, the training loop shuffles the training split with a seed-specific NumPy RNG, optimizes with AdamW, validates on the validation split each epoch, saves the best validation checkpoint, and reloads that checkpoint for downstream evaluation and diagnostics. The scheduler monitors validation position MSE. Training was configured for at most 120 epochs with early-stopping patience 24. In the completed fixed-horizon scale/OOD evaluation, all recorded training curves reached epoch 120:

Variant	Architecture	Seed	Final epoch	Final val position MSE
kinematic_only	GRU-R2h-loss-long	3407	120	0.000294534
kinematic_only	GRU-R2h-loss-long	3408	120	0.000236122
kinematic_only	RSSM-large-position-heavy-long	3407	120	0.00012529

kinematic_only	RSSM-large-position-heavy-long	3408	120	0.000135432
kinematic_only	Transformer-lite full-pass configuration	3407	120	0.000117449
kinematic_only	Transformer-lite full-pass configuration	3408	120	0.000129377
observation_like	GRU-R2h-loss-long	3407	120	0.000297152
observation_like	GRU-R2h-loss-long	3408	120	0.000204312
observation_like	RSSM-large-position-heavy-long	3407	120	0.000162925
observation_like	RSSM-large-position-heavy-long	3408	120	0.000178298
observation_like	Transformer-lite full-pass configuration	3407	120	9.46372e-05
observation_like	Transformer-lite full-pass configuration	3408	120	0.000160981

A.3 Hidden-state extraction

Hidden states are extracted during evaluation through the shared fixed-horizon evaluation function. For each batch, the model returns $(\text{prediction}, \text{embedding})$. The evaluation function accumulates predictions and embeddings without gradient tracking and computes position MSE against the future target positions.

The hidden-state definition is architecture-specific but standardized as the returned embedding:

- `GRU-R2h-loss-long`: the final recurrent hidden state of the top GRU layer.
- `Transformer-lite full-pass configuration`: the final-token encoder representation after the transformer encoder.
- `RSSM-large-position-heavy-long`: the latent state produced by the posterior/transition stack.

The extracted train embeddings are used for event-probe fitting. The extracted test/ID/OOD embeddings are used for event-probe evaluation, and diagnostic comparisons. Evaluation uses batch size 128 and runs on CUDA if available, otherwise CPU.

A.4 Event probe

The event probe is a lightweight linear classifier trained on model hidden states to classify event family: free motion, collision, or occlusion. It is used only as an event-regime readout diagnostic. It does not prove that the model causally uses the event representation.

The implemented probe standardizes train and test embeddings using the training embedding mean and standard deviation. Probe weights are initialized from a normal distribution with standard deviation 0.01, and the bias is initialized to zero. The classifier is optimized with full-batch gradient descent for 500 iterations with learning rate 0.08 and L2 weight penalty 10^{-4} . Reported metrics include accuracy, macro-F1, balanced accuracy, majority baseline, and per-class precision/recall/F1.

The baseline evaluation reports event-probe macro-F1 on the ID test split. The main sanity table reports event-probe macro-F1 = 1.000 for all kinematic-only architecture/seed rows:

Variant	Architecture	Seed	ID_MSE	CV_MSE	Probe F1	CFE collision
kinematic_only	GRU-R2h-loss-long	3407	2.46E-04	3.35E-04	1	9.42E-05
kinematic_only	Transformer-lite full-pass configuration	3407	9.98E-05	3.35E-04	1	1.60E-04
kinematic_only	RSSM-large-position-heavy-long	3407	1.49E-04	3.35E-04	1	7.21E-04
kinematic_only	GRU-R2h-loss-long	3408	2.23E-04	3.35E-04	1	7.12E-05
kinematic_only	Transformer-lite full-pass configuration	3408	1.21E-04	3.35E-04	1	1.36E-04
kinematic_only	RSSM-large-position-heavy-long	3408	1.40E-04	3.35E-04	1	7.70E-04

A.5 Original fixed-horizon CFE audit baseline and suppression sweep

The Causal Field Effect (CFE) measures causal sensitivity by modifying hidden representations and decoding predictions from the modified hidden state. In the original fixed-horizon baseline CFE score, event-specific examples are selected by mask, the model predicts the future target, and the baseline position MSE

is measured. The hidden embedding is centered, partially suppressed, decoded through the model head, and evaluated again. In that original baseline implementation, CFE is defined as:

$$\text{CFE} = \text{perturbed_position_mse} - \text{baseline_position_mse}.$$

Positive CFE means the perturbation increased event-relevant prediction error. This is causal sensitivity evidence, not complete mechanism identification.

The baseline implementation additionally performs a suppression-strength sweep. The strengths are 0.25, 0.5, 0.75, 1.0. The implemented sweep compares four intervention/control modes:

- `target_field_suppression`: suppresses the centered target embedding by the requested strength.
- `matched_norm_random_direction`: subtracts a random direction scaled to match the centered embedding standard deviation.
- `field_label_shuffle`: suppresses shuffled centered embeddings.
- `random_subspace_control`: suppresses a random binary subspace of the centered embedding.

The sweep is run for two diagnostic fields. `CFE_collision` uses the kinematic-only variant on the collision OOD split. `CFE_hard_occlusion` uses the observation-like variant on the hard-occlusion OOD split. The generated baseline suppression-sweep table contains 192 rows:

Field	Control	Rows
CFE_collision	field_label_shuffle	24
CFE_collision	matched_norm_random_direction	24
CFE_collision	random_subspace_control	24
CFE_collision	target_field_suppression	24
CFE_hard_occlusion	field_label_shuffle	24
CFE_hard_occlusion	matched_norm_random_direction	24
CFE_hard_occlusion	random_subspace_control	24
CFE_hard_occlusion	target_field_suppression	24

The original baseline CFE sweep should be interpreted conservatively. It is useful as an audit baseline and as implementation history, but it is not the source definition for the Figure 2 results in the main text. Dose sensitivity in this baseline sweep supports causal diagnostic evidence, but controls such as field-label shuffle can be non-negligible because hidden-state factors are correlated. Therefore, the original baseline CFE sweep does not prove a complete causal mechanism.

A.6 Relationship to the reported fixed-horizon projection CFE

The main CFE evidence reported in Section 6.3 and Figure 2 uses the reinforced fixed-horizon windowed projection CFE described mathematically in Appendix C. That analysis differs from the original baseline

CFE sweep in three important ways: it evaluates explicit event windows after intersecting them with the configured future prediction horizon; it derives field directions from a trained linear readout using a probe-logit-contrast direction; and it performs one-dimensional projection suppression in the same normalized hidden-state space used by the readout before decoding perturbed predictions.

Code and data availability. The public release contains the training code, model definitions, diagnostic scripts, figure-generation scripts, dataset manifest, result tables, and non-primary audit materials used to support the manuscript. The detailed file-level mapping between manuscript results and repository artifacts is provided in the GitHub repository.

Appendix B. Mathematical Details for Figure 1

This appendix defines the quantities plotted in Figure 1. Panels A, D, and E use hidden-state field readout scores; Panels B and C use data-level proxy z-scores; and Panel F uses positive shift fractions from a lighter sliding-prefix analysis. These quantities should be compared within each panel, not across panels.

B.1 Hidden-state field readout scores for Panels A, D, and E

Let $x \in \mathbb{R}^d$ denote a hidden state from the model representation being analyzed. We use three field labels: K for kinematic, C for contact, and O for object-permanence. Let $\mathcal{F} = \{K, C, O\}$ denote this label set. Before applying the field readout, the hidden state is standardized using the training-set mean and standard deviation used for probe training:

$$h_{\text{norm}} = \frac{h - \mu_{\text{train}}}{\sigma_{\text{train}}}.$$

The standardization is applied elementwise. The field readout is a trained 3-class linear probe. It computes field logits as

$$\ell = Wh_{\text{norm}} + b, \quad W \in \mathbb{R}^{3 \times d}, \quad b \in \mathbb{R}^3.$$

Here W and b are the learned weight matrix and bias vector of the linear probe, not parameters of the transition model. The three output dimensions of ℓ correspond to K , C , and O . Equivalently, for field label f ,

$$\ell_f = w_f^T h_{\text{norm}} + b_f,$$

where w_f is the row of W associated with field label f . The probe is trained on the training split with a cross-entropy objective and then frozen for the Figure 1 analyses.

The plotted hidden-state field readout score is the softmax probability assigned to field label f :

$$s_f(x) = \frac{\exp(\ell_f - m)}{\sum_{g \in \mathcal{F}} \exp(\ell_g - m)}, \quad m = \max_{g \in \mathcal{F}} \ell_g.$$

The subtraction of m is a numerically stable implementation of the standard softmax and does not change the probability. The scores over the three fields sum to one for each hidden state. Thus, $s_f(h)$ measures the relative probability mass assigned by the trained probe to field label f for that hidden state. It should be interpreted as a readout-assigned field emphasis, not as an absolute physical intensity.

Panel A aggregation

Panel A summarizes event-level field emphasis. Let \mathcal{J}_e be the set of held-out sequences belonging to event family e , and let \mathcal{T}_i denote the set of hidden states from sequence i included in the event-level aggregation.

The event-level score for field label f is

$$S_{e,f} = \frac{1}{|\mathcal{J}_e|} \sum_{i \in \mathcal{J}_e} \left(\frac{1}{|\mathcal{J}_i|} \sum_{t \in \mathcal{J}_i} s_f(h_{i,t}) \right).$$

If a sequence-level or final hidden representation is used, \mathcal{J}_i contains that representation. If multiple time entries are used, the probability is first averaged within sequence/time entries and then averaged across sequences in the same event family.

Panels D and E aligned-time aggregation

Panels D and E summarize time-aligned hidden-state dynamics. For a sequence i , let b_i denote the event boundary used for alignment: the contact onset for collision and hidden-start for occlusion. For relative time τ , the aligned field score is

$$S_f(\tau) = \frac{1}{|\mathcal{J}(\tau)|} \sum_{i \in \mathcal{J}(\tau)} s_f(h_{i,b_i+\tau}),$$

where $\mathcal{J}(\tau)$ is the set of sequences for which the aligned time $b_i + \tau$ is available. When multiple seeds are plotted, the curve is computed per seed and then summarized by the mean across seeds; error bars, when shown, represent the corresponding standard error of the mean.

B.2 Data-level proxy z-scores for Panels B and C

Panels B and C are not hidden-state readouts. They describe the physical demands of annotated event phases using data-level proxies derived from object states, pairwise relations, event-phase labels, and visibility/contact annotations. Kinematic proxies summarize motion-related quantities such as displacement, velocity, or visible trajectory structure. Contact proxies summarize pairwise interaction or contact-related structure. Object-permanence proxies summarize occlusion, hidden-state, or reappearance-related demands.

Let $r_{f,\phi}$ denote the raw data-level proxy value for field label f in phase ϕ . For the collision panel, phases include pre-contact, contact, and post-contact. For the occlusion panel, phases include pre-occlusion, hidden, and reappearance when that phase is available in the selected analysis table. The raw field-by-phase proxy matrix is standardized within each panel:

$$\mu_{\text{panel}} = \frac{1}{|\mathcal{F}||\Phi|} \sum_{f \in \mathcal{F}} \sum_{\phi \in \Phi} r_{f,\phi},$$

$$\sigma_{\text{panel}} = \sqrt{\frac{1}{|\mathcal{F}||\Phi|} \sum_{f \in \mathcal{F}} \sum_{\phi \in \Phi} (r_{f,\phi} - \mu_{\text{panel}})^2},$$

$$z_{f,\phi} = \frac{r_{f,\phi} - \mu_{\text{panel}}}{\sigma_{\text{panel}}}.$$

Thus, $z_{f,\phi}$ indicates whether a proxy-defined field demand is relatively high or low within that panel. These proxy z-scores are used to interpret the physical structure of the trajectory itself. They do not imply that the model hidden state activates the corresponding field.

B.3 Positive shift fractions and directional consistency for Panel F

Panel F summarizes the lighter sliding-prefix hidden-state analysis for GRU and Transformer-lite. Unlike the RSSM rollout-latent analysis in Panels D and E, this analysis does not reconstruct full phase-resolved hidden dynamics. It only asks whether the expected field score changes in the expected direction for each evaluated case.

Let \mathcal{C} be the set of evaluated cases, such as architecture-seed-variant combinations. For each case c , hidden states are extracted from sliding prefixes, and the same field-score logic is used to obtain $s_f(h)$ for the relevant prefix-conditioned hidden states.

For collision, the expected effect is a positive shift in the contact score around the contact/collision phase relative to an earlier baseline phase. Define

$$\bar{s}_{\mathcal{C},\text{target}}^c = \text{mean}_{(i,t) \in W_{\text{contact}}^c} s_{\mathcal{C}}(h_{i,t}^c),$$

$$\bar{s}_{\mathcal{C},\text{base}}^c = \text{mean}_{(i,t) \in W_{\text{pre-contact}}^c} s_{\mathcal{C}}(h_{i,t}^c),$$

and

$$\Delta_{\mathcal{C}}^c = \bar{s}_{\mathcal{C},\text{target}}^c - \bar{s}_{\mathcal{C},\text{base}}^c.$$

For occlusion, the expected effect is a positive shift in the object-permanence score during the hidden/occlusion phase relative to a pre-occlusion baseline. Define

$$\bar{s}_{\mathcal{O},\text{target}}^c = \text{mean}_{(i,t) \in W_{\text{hidden}}^c} s_{\mathcal{O}}(h_{i,t}^c),$$

$$\bar{s}_{\mathcal{O},\text{base}}^c = \text{mean}_{(i,t) \in W_{\text{pre-occlusion}}^c} s_{\mathcal{O}}(h_{i,t}^c),$$

and

$$\Delta_{\mathcal{O}}^c = \bar{s}_{\mathcal{O},\text{target}}^c - \bar{s}_{\mathcal{O},\text{base}}^c.$$

Here \mathcal{C} denotes the contact field label and \mathcal{O} denotes the object-permanence field label. The windows W_{contact}^c , W_{hidden}^c , $W_{\text{pre-contact}}^c$, and $W_{\text{pre-occlusion}}^c$ follow the phase labels available in the sliding-prefix analysis tables.

For each evaluated case, we convert the two shifts into directional indicators:

$$I_C^c = \mathbf{1}[\Delta_C^c > 0], \quad I_O^c = \mathbf{1}[\Delta_O^c > 0].$$

For an architecture group $A \subseteq \mathcal{C}$, the positive shift fractions are

$$\text{PSF}_A^C = \frac{1}{|A|} \sum_{c \in A} I_C^c, \quad \text{PSF}_A^O = \frac{1}{|A|} \sum_{c \in A} I_O^c.$$

The joint directional consistency score aggregates the two expected shifts across all evaluated cases:

$$\text{DCS} = \frac{1}{2|\mathcal{C}|} \sum_{c \in \mathcal{C}} (I_C^c + I_O^c).$$

Panel F reports these positive shift fractions and the joint DCS. A value of 1.000 means that every evaluated case showed the expected positive direction. This supports directional consistency in prefix-conditioned hidden states, but it should not be interpreted as full time-resolved rollout dynamics or as evidence of explicit field modules.

B.4 Interpretation boundary

The Figure 1 quantities have different scales and should not be compared across panels. Panels A, D, and E report softmax probabilities from hidden-state readouts; Panels B and C report standardized data-level proxy values; Panel F reports fractions of positive directional shifts. The intended interpretation is event-conditioned reweighting of non-exclusive diagnostic fields. The results do not establish one-to-one event-to-field assignment, explicit field modules, or a complete mechanistic decomposition.

Appendix C. Mathematical and Implementation Details for Causal Field Effects

This appendix defines the causal field effect (CFE) quantities used in Section 6.3. The reported implementation uses **fixed-horizon, windowed projection CFE**. Event windows are evaluated only where they overlap the configured future prediction horizon. This means that CFE is computed only on frames for which the base model and the perturbed model both produce predictions.

C.1 Notation and fixed-horizon event windows

Let c index an evaluated case, such as an architecture-seed-variant combination. Let i index a sequence, t index a predicted frame, o index an object, and $d \in \{x, y\}$ index the position coordinate used in the CFE loss. The transition model produces a hidden representation h_i^c or $h_{i,t}^c$, depending on the architecture-specific interface, and a prediction $\hat{y}_{i,t,o,d}^c$ for the target state $y_{i,t,o,d}$.

For compact notation, let

$$\mathcal{F} = \{K, C, P\}$$

where K denotes the kinematic field, C denotes the contact field, and P denotes the object-permanence field.

Let T_{future} denote the fixed set of frames predicted by the model. In the reported experiments, the model observes the first eight frames and predicts the next eight frames, so the prediction horizon corresponds to the configured future target frames. Let $\tilde{W}_e(i)$ denote the event-defined raw window for event family e in sequence i . The implemented CFE window is the intersection of the event-defined window and the predicted future horizon:

$$W_e(i) = \tilde{W}_e(i) \cap T_{\text{future}}$$

Equivalently, the implemented window contains exactly those frames that are both event-relevant and predicted by the model:

$$t \in W_e(i) \Leftrightarrow t \in \tilde{W}_e(i) \text{ and } t \in T_{\text{future}}$$

For collision, $W_e(i)$ is centered on the contact regime after this intersection. For hard occlusion, the primary CFE window covers hidden frames within the predicted horizon. The current primary analysis does not report a reappearance-window CFE, because no reappearance frames remain in the configured fixed-horizon CFE window.

C.2 Base event-window prediction loss

The base prediction loss is computed without intervention. The reported CFE loss is normalized x/y position MSE over the selected sequence-frame-object-coordinate entries. For an event family e and case c , define the set of evaluated sequences as I_e^c . Let

$$N_e^c = \sum_{i \in I_e^c} \sum_{t \in W_e(i)} \sum_o \sum_{d \in \{x,y\}} 1$$

be the number of evaluated sequence-frame-object-coordinate entries. The base event-window loss is

$$L_{\text{base}}^c(e) = \frac{1}{N_e^c} \sum_{i \in I_e^c} \sum_{t \in W_e(i)} \sum_o \sum_{d \in \{x,y\}} (\hat{y}_{i,t,o,d}^c - y_{i,t,o,d})^2$$

Thus, the base loss is not a full-state loss over all target channels. It is the normalized position-prediction loss in the fixed-horizon event window.

C.3 Field-direction construction from the linear readout

The field directions used for projection suppression are derived from the trained 3-class linear field readout. Given a hidden representation h , we first apply the same training-set normalization used by the readout:

$$z = \frac{h - \mu_{\text{train}}}{\sigma_{\text{train}}}$$

The readout produces logits

$$\ell = Wz + b$$

where $W \in \mathbb{R}^{3 \times d}$ is the learned weight matrix, $b \in \mathbb{R}^3$ is the learned bias vector, and the three output dimensions correspond to K , C , and P . Let w_f denote the row of W associated with field f . For the reported probe_logit_contrast direction, we compute

$$v_f = w_f - \frac{1}{|\mathcal{F}| - 1} \sum_{g \in \mathcal{F}, g \neq f} w_g$$

The unit field direction is

$$u_f = \frac{v_f}{\|v_f\|_2}$$

This direction should be interpreted as a readout-aligned representational direction, not as a unique physical module. In a multi-class readout, field evidence is relative, and readout directions can overlap with other predictive structure.

C.4 Projection suppression intervention

Let $A_{f,\alpha}$ denote the intervention that suppresses the component of the normalized hidden representation associated with field f at suppression strength α . The reported sweep evaluates

$$\alpha \in \{0.25, 0.50, 0.75, 1.00\}$$

For one-dimensional projection suppression, the perturbed normalized representation is

$$z^{(-f, \alpha)} = A_{f, \alpha}(z) = z - \alpha (z^\top u_f) u_f$$

The operator $A_{f, \alpha}$ should be interpreted as a representational-subspace intervention. It suppresses a readout-aligned direction; it does not prove that the model contains an explicit field module or isolated causal circuit.

The perturbed representation is then mapped back to the model’s hidden-state scale using the inverse of the readout normalization:

$$h^{(-f, \alpha)} = \mu_{\text{train}} + \sigma_{\text{train}} \odot z^{(-f, \alpha)}$$

C.5 Perturbed prediction loss and CFE

After intervention, the perturbed hidden representation is decoded to obtain perturbed predictions $\hat{y}_{i,t,o,d}^{c,(-f, \alpha)}$.

For GRU and Transformer-lite, the perturbed representation is decoded through the corresponding prediction head. For RSSM-lite in the reported analysis, CFE is computed by head decoding from the perturbed latent state; it is not a full RSSM transition re-rollout intervention.

The perturbed event-window loss is

$$L_{\text{pert}}^c(e, f, \alpha) = \frac{1}{N_e^c} \sum_{i \in I_e^c} \sum_{t \in W_e(i)} \sum_o \sum_{d \in \{x, y\}} \left(\hat{y}_{i,t,o,d}^{c,(-f, \alpha)} - y_{i,t,o,d} \right)^2$$

The causal field effect is the event-window loss increase caused by the field-aligned intervention:

$$\text{CFE}^c(e, f, \alpha) = L_{\text{pert}}^c(e, f, \alpha) - L_{\text{base}}^c(e)$$

A positive CFE means that suppressing the field-aligned component worsens prediction in the evaluated event window. Let e_{col} denote the collision-contact window and e_{hid} denote the hard-occlusion hidden window. The two primary CFE quantities used in Section 6.3 are

$$\text{CFE}_{\text{col}}^c(\alpha) = \text{CFE}^c(e_{\text{col}}, C, \alpha)$$

$$\text{CFE}_{\text{hid}}^c(\alpha) = \text{CFE}^c(e_{\text{hid}}, P, \alpha)$$

The current primary analysis should not be described as reappearance-window CFE. When CFE is reported without specifying a suppression-strength sweep, it refers to the configured suppression strength for that summary, typically $\alpha = 1$.

C.6 Aggregation across cases

For a set of evaluated cases \mathcal{C} , such as all architecture-seed combinations, the mean CFE at event e , target

field f , and strength α is

$$\overline{\text{CFE}}(e, f, \alpha) = \frac{1}{|\mathcal{C}|} \sum_{c \in \mathcal{C}} \text{CFE}^c(e, f, \alpha)$$

When plotted, error bars or standard errors can be computed over the same set of cases. In the main text, the sign of the effect, target-control comparison, and dose trend are more important than the absolute magnitude of any single loss delta.

C.7 Matched controls and target-control margins

CFE is interpreted relative to matched controls. Let q denote a control intervention type. The controlled CFE is

$$\text{CFE}_q^c(e, f, \alpha) = L_{\text{pert},q}^c(e, f, \alpha) - L_{\text{base}}^c(e)$$

The main controls are matched-norm random direction, random subspace control, field-label shuffle. A useful target-control margin is

$$M_q(e, f, \alpha) = \overline{\text{CFE}}_{\text{target}}(e, f, \alpha) - \overline{\text{CFE}}_q(e, f, \alpha)$$

Positive margins indicate that target-field suppression degrades prediction more than the corresponding control. The interpretation is comparative: a positive target CFE without positive margins may indicate general perturbation sensitivity rather than field-specific functional relevance. Conversely, negative or weak margins should be interpreted as reduced specificity, not as evidence for an explicit module.

C.8 Suppression-strength sweep

The suppression sweep evaluates whether CFE increases as the intervention becomes stronger. For strengths $\alpha_1 < \alpha_2$, a dose-sensitive pattern satisfies

$$\text{CFE}(e, f, \alpha_2) \geq \text{CFE}(e, f, \alpha_1)$$

for most adjacent strength pairs and evaluated cases. Perfect monotonicity is not required, because finite samples, different architectures, and overlapping field directions can introduce deviations. The relevant pattern is a broadly dose-sensitive increase in event-window prediction loss under stronger target-field suppression, interpreted together with matched controls.

C.9 Interpretation boundary

CFE is a functional relevance measure within the configured prediction setting, not a full causal-mechanistic explanation. It supports the claim that field-aligned representational structure has predictive consequences

in the relevant fixed-horizon event window. It does not establish that the model contains an explicit physical module, that the intervention isolates a unique circuit, that the RSSM transition has been fully re-rolled under intervention, or that the result generalizes to arbitrary sliding-context forecasts.

The strongest supported interpretation is therefore: field-aligned components are functionally relevant when suppressing them selectively increases prediction loss in the fixed-horizon event window where that field is expected to matter, relative to matched controls.

C.10 Summary of the empirical pattern

The core expected pattern is positive collision-contact CFE and positive hard-occlusion hidden-window CFE, together with appropriate controls:

$$CFE_{\text{col}}(\alpha) > 0$$

$$CFE_{\text{hid}}(\alpha) > 0$$

Reappearance-window CFE is not part of the current primary result. Together with positive target-control margins and broadly dose-sensitive suppression trends, these results support fixed-horizon functional sensitivity of contact and object-permanence field-aligned components in the event regimes where they are expected to matter. The evidence should not be phrased as explicit physical modules, isolated causal circuits, full RSSM rollout interventions, or arbitrary sliding-context generalization.